ECMWF – ARM Report Series

4. Evaluation of trade cumulus and the DualM parameterization in the ECMWF model

M. Ahlgrimm, M. Köhler

European Centre for Medium-Range Weather Forecasts
Europäisches Zentrum für mittelfristige Wettervorhersage
Centre européen pour les prévisions météorologiques à moyen terme

Series: ECMWF - ARM Report Series

A full list of ECMWF Publications can be found on our web site under:
http://www.ecmwf.int/publications/

Contact: library@ecmwf.int

European Centre for Medium Range Weather Forecasts
Shinfield Park, Reading, RG2 9AX, England

ECMWF - ARM Report Series No. 4

Evaluation of trade cumulus and the DualM parameterization in the ECMWF model

M. Ahlgrimm[1] and M. Köhler

Dec 2009

Submitted to Monthly Weather Review

[1]Fellowship sponsored by ARM

Abstract

CALIPSO observations are used to assess trade cumulus cloudiness in three versions of the Integrated Forecasting System of the European Centre for Medium-Range Weather Forecasts. The observations are recast onto the model grid, and two simple threshold criteria for cloud top height and cloud fraction are used to identify grid points containing trade cumulus clouds. The cloud fraction and top height distributions of the sample populations are then compared. Results show that all versions of the model overestimate the frequency of occurrence of trade cumulus clouds, but underestimate their cloud fraction when present. These effects partially compensate. Cloud top heights are overestimated in model cycles using the modified Tiedtke parameterization for shallow convection, but are in very good agreement with observations when the Dual Mass Flux parameterization is introduced.

1 Introduction

In his 1999 paper, Jakob (1999) found that the Integrated Forecasting System (IFS) as used for the ECMWF 40-year re-analysis (Uppala et al., 2005) underestimates marine stratocumulus cloud cover by 15%, but overestimates the cloud cover in the trade cumulus regions by 10-15%. The current cloud scheme in the IFS is still based on the same prognostic Tiedtke scheme (Tiedtke, 1993) with some modifications over time (Jung et al., 2009). While the representation of stratocumulus clouds improved markedly with the introduction of the Eddy Diffusivity Mass Flux parameterization (Köhler, 2005; Tompkins et al., 2004; Ahlgrimm et al., 2009), the model still shows evidence of a cloud cover bias in the trade cumulus regions.

Ongoing evaluation of the model's top-of-the-atmosphere shortwave fluxes against CERES measurements suggests that the model is too reflective in the trade cumulus regions. However, it is difficult to separate errors in cloud optical properties, cloud amount and frequency of occurrence from these long-term runs. As suggested by Jakob (2003), compositing based on pre-defined atmospheric conditions can be a helpful intermediate between the evaluation of model climate, where the link to individual model components is often not obvious, and case studies, which may not be sufficiently representative. The study presented here follows such an intermediate path by using global observations from CALIPSO, defining criteria that select samples containing trade cumulus clouds and comparing the properties of the observed and modeled sample populations. CALIPSO provides a very accurate estimate of cloud top height, as well as an along-track cloud fraction, and the frequency with which samples are found.

Section 2 describes the observations used for this evalution, while section 3 introduces the model cycles and briefly summarizes the changes implemented from one cycle to the next. The methods used to compare model results with observations are explained in section 4. The use of profiler observations with a narrow footprint to estimate cloud cover over an area is always subject to a sampling error. In section 5, the impact this error may have on the results of this study is explored. Section 6 concludes this article.

2 CALIPSO observations

CALIPSO observes cloud and aerosol layers with very high vertical and along-track resolution. In the lower troposphere, individual footprints are spaced 333 m apart, and vertical bins measure 30 m. Full signal attenuation occurs in features with an optical depth greater than approximately three. Thus, the signal is frequently attenuated in marine boundary layer clouds, and a cloud base retrieval is unreliable. For this study, the level 2 cloud layer product at 1 km horizontal resolution is used. For this product, three individual backscatter profiles are averaged before searching for cloud layers. This improves the signal-to-noise ratio, while still maintaining

	CY31R1	CY32R3	CY32R3-DM
Name	pre-ERA-I	McICA	DualM
Shallow convection param.	modified Tiedtke	modified Tiedtke	Dual Mass Flux
Boundary layer param.	EDMF	EDMF	Dual Mass Flux
Operational period	12 Sep 2006 - 12 Dec 2006	6 Nov 2007 - 11 Mar 2008	experimental

Table 1: ECMWF model cycles.

a high along-track resolution (Vaughan et al., 2005). Each 1 km average profile is flagged for full signal attenuation. Data from six months (January 2007, 2008, 2009 and July 2006, 2007, 2008) are compared to model results from three versions of the IFS.

3 Model cycles

The three model cycles in this comparison were chosen because they mark changes in the model physics with potential impact on the low cloud cover. Table 1 lists the model cycle names and periods during which the cycles were operational. The oldest cycle considered, CY31R1, is the cycle just previous to the model version used in the ECMWF interim reanalysis (Simmons et al., 2007) and uses the same physics package. Changes in the model physics from the ECMWF 40-year reanalysis to CY31R1 are described in Beljaars et al. (2006). It uses the Eddy-Diffusivity Mass Flux (EDMF) parameterization to model boundary layer processes and stratocumulus clouds. Shallow and deep convection are parameterized using Tiedtke's method (Tiedtke, 1989).

In CY32R3, the Monte Carlo independent column approximation (McICA) is implemented and the model's shortwave radiation is replaced by the rapid radiative transfer model RRTM-SW (Iacono et al., 2008). In addition, the convection parameterization for deep convection is updated and vertical diffusion in the free atmosphere reduced (Bechtold et al., 2008).

The last cycle considered is a modified version of CY32R3. The EDMF dry and stratocumulus topped boundary layer parameterization operational at ECMWF since April 2005 is now under development to be upgraded to include shallow cumulus. Neggers et al. (2009) proposed a dual mass-flux description (DualM) to allow the freedom to describe non-local parcels reaching cloud base and cloud top separately, but in an integral framework. Work towards implementation has required a few upgrades to the published work, which are summarized in the Appendix. The Dual Mass Flux parameterization replaces the Tiedtke scheme for shallow convection originating in the surface layer. The Tiedtke scheme is still used to represent shallow convection originating above the surface layer, allowing multi-level triggering.

In all cases, the IFS is run at T399 (approximately 50 km) resolution with 91 vertical levels. The forecasts are initialized at 00 UTC every other day and run for three consecutive days. The first 24 hours of each forecast are discarded, and days two and three of each forecast are stitched together to provide a month-long continuous record. All forecasts are initialized from the operational analysis current for the year and month of the run (Table 2). No appreciable spinup of the forecasts is apparent in the trade cumulus cloud fields after the first 12-24 hours, as will be shown in the results section.

Month	Cycle of operational analysis
Jul 2006	CY30R1
Jan 2007	CY32R2
Jul 2007	CY32R2
Jan 2008	CY32R3
Jul 2008	CY33R1
Jan 2009	CY35R1

Table 2: Operational analyses that were used to initialize model runs.

4 Method

Two simple threshold criteria for cloud fraction and top height are used to independently identify samples containing trade cumulus clouds in model and observations. The search area is restricted to the ocean between $30^{\circ}N$ and $30^{\circ}S$. The frequency of occurrence, cloud top height and cloud fraction of these samples is then compared.

For an equitable comparison of CALIPSO observations with the model, the observations are first recast onto the model grid. The level 2, 1 km layer products used here provide the cloud top and base height for each observed cloud layer, as well as the information whether the cloud fully attenuated the lidar signal. The strategy for determining vertically resolved cloud fraction on the model grid and a column-representative cloud top height follows the steps outlined in Ahlgrimm et al. (2009). To summarize, in each model layer, the ratio of cloudy lidar shots to the total number of shots falling into the model column provides an along-track cloud fraction. The column-representative cloud top height is an average of all observed cloud tops associated with the lowest cloud feature in the column. If this cloud-top height does not exceed 4 km, and the cloud fraction remains below 50%, the sample is considered to contain trade cumulus (TCu) clouds. Over a month, the lidar samples about 96,000 ocean grid points within the prescribed region.

In the model, cloud fraction is a prognostic variable and readily available. In order to calculate a cloud-top height representative of the lowest modeled cloud feature in the column, the generalized overlap assumption (Räisänen et al., 2004) is used to create binary subcolumns. The number of subcolumns is equal to the number of lidar shots within the grid box. The column-representative cloud top height is calculated equivalent to the observations from the "cloud tops" of the subcolumns. Cloud edges always fall onto model layer interfaces, consistent with the assumption that clouds fill model layers homogenously in the vertical.

A lidar simulator is used to determine whether the clouds in the subcolumns fully attenuate the lidar signal. This simulator is based on Chiriaco et al. (2006) with modifications. Particle effective radii are calculated from cloud liquid and ice water contents consistent with the IFS short wave code of cycle CY32R3. Where the model does not provide guidance, constants and parameters are chosen as in the CFMIP Observation Simulator Package v 1.0 (available from www.cfmip.net). The simulated level of signal attenuation is used to adjust the subcolumn cloud base to an apparent cloud base where full attenuation occurs. However, the simulated backscatter signal is not used to identify cloud layers from the model. In the absence of aerosol and artificial noise (which are not included in the simulator), the simulated backscatter for lower tropospheric clouds always exceeds the molecular background such that the resulting cloud field is identical to the binary subcolumns used as input for the simulator. Parallel to the observations, the model samples, using the attenuation-corrected cloud fraction, are compared to the critical values for cloud fraction and top height and labeled TCu when appropriate.

5 Results

5.1 Distributions

Figure 1 shows distributions of cloud fraction (left column) and column-representative cloud top height (right column) of CALIPSO samples classified as TCu for the three months of July. The sample distributions are very similar for all three Julys. In all cases, around 45% of samples fulfill the cloud fraction and top-height criteria for trade cumulus. Out of those samples, approximately 30% of individual 1 km profiles are fully attenuated, i.e. contain clouds with optical depth of more than approximately 3. The panels in the left column show that along-track cloud fractions are most frequently observed in the 10-20% range, with slighly decreasing sample numbers for higher and lower fractions. The right panel shows the cloud top height distribution of the TCu samples as a sample density. Since cloud boundaries in the model always fall onto model layer interfaces, irregular bins whose width corresponds to the model layer thickness are used in this distribution. The vertical axis shows the sample density within each bin as number of samples per width of the bin (m^{-1}). The peak of this distribution is located around 850 m with a skewed tail towards higher cloud tops: Shallow clouds topping out around 850 m are observed most frequently, while deeper clouds occur less often.

Figure 2 shows the corresponding distributions for IFS cycle CY31R1. From here on, only July 2008 is shown, as all months look very similar and percentages do not differ by more than 1%. The cloud top height distribution from CALIPSO is plotted in dark grey in the background of the right panel, for easier comparison. About 70% of the samples are classified as TCu in the model, significantly more than the 45% observed. Samples with less than 10% cloud fraction are most common, with sample numbers decreasing with increasing cloud fraction. Compared to CALIPSO, it appears that most of the additional samples found in the model have small (¡20%) cloud fraction. The peak in the cloud top height distribution can be found near 1500 m, and the distribution is less skewed. The lidar simulator determines 63% of the subcolumns to be fully attenuated in the TCu samples.

The picture is similar for CY32R3 (Figure 3, top row). In this cycle, slighly fewer samples are classified as TCu (65%), but still significantly more than observed. The cloud fraction distribution has a similar emphasis on small fractions, and cloud tops are too high. The cloud top height distribution has a slightly lower peak than previously and is more skewed, overestimating the occurrence of deeper clouds.

The cloud top height distribution is improved markedly by the introduction of the DualM parameterization (Fig. 3). The low level peak agrees very well with the CALIPSO observations, though the occurrence of deeper clouds is still overestimated. Unfortunately, the occurrence of clouds with very low fraction increases again to 71%.

Results for January 2007 (Figure 4) are very similar to the other Januarys and the months of July. Trade cumulus clouds are found with the same frequency and characteristics in observation and model, albeit in slightly different areas of the globe. The similarity of the distributions between months and seasons suggests that sample classification reliably identifies clouds with similar characteristics, regardless of season or exact location.

To ensure that clouds from forecast days two and three do not differ due to model spinup, samples have been split according to model forecast day in Figure 5. Half the samples (from model forecast day two) are shown in the black curve, while the other half (from forecast day three) are shown in dark grey. No systematic shift in the curves or number of samples is apparent, confirming that sample populations are similar for forecast days two and three. It also shows that even half a month of observations is a sufficiently long time collect a robust sample population.

The shift in the cloud top height distribution from CY32R3 to CY32R3-DM can be traced back to aspects of

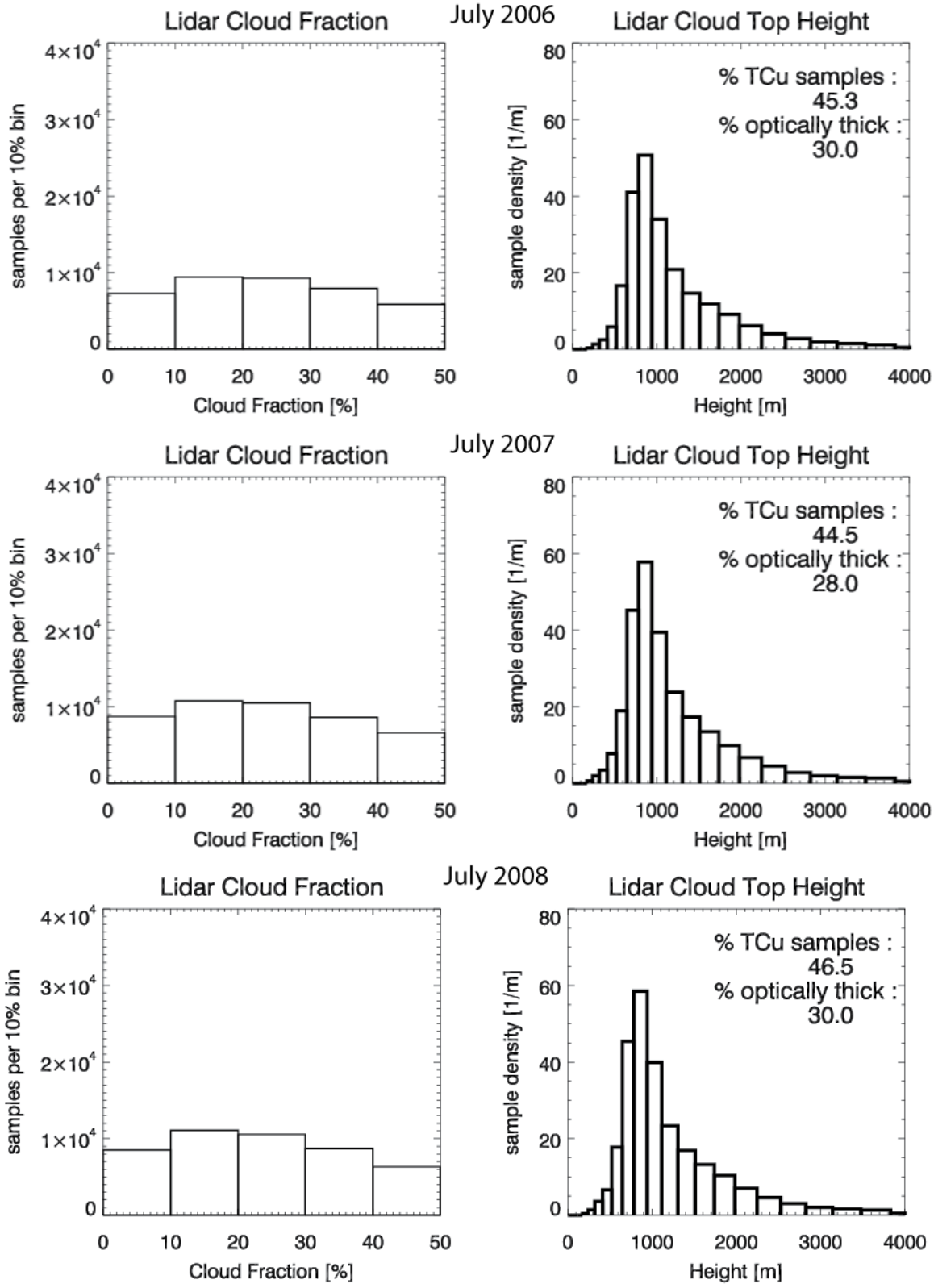

Figure 1: CALIPSO cloud fraction (left) and cloud top height (right) distributions for July 2006, 2007 and 2008.

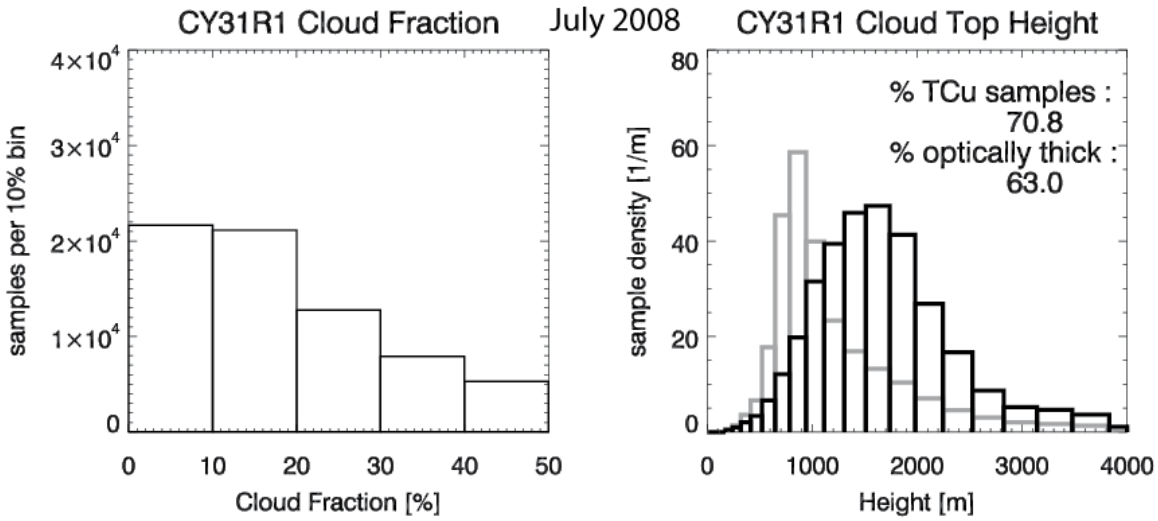

Figure 2: Cloud fraction and cloud top height distributions for model cycle CY31R1 for the month of July 2008.

the Tiedtke scheme for shallow convection and the Dual Mass Flux parameterization. In the modified Tiedtke formulation as used in CY32R3, the volume of the updraft is conserved, and the updraft mass is detrained in the upper half of the cloud. The detrained cloud volume appears as a source term in the model's prognostic equation for cloud fraction. Almost invariably, this leads to "top heavy" clouds in the trade regions. The greatest cloud fractions in the model column are found in the upper half of the cloud, with small cloud fractions at cloud base (Figure 6). The DualM parameterization was developed and tested based on observational campains such as BOMEX (Siebesma et al., 2003) which suggest that cloud cover and mass flux are greatest at cloud base and decrease with height in the undisturbed trade wind regime. The DualM parameterization reproduces this profile well and indeed places the greatest cloud fractions at cloud base. When the model column is divided into subcolumns, the difference in the cloud fraction profiles translates into a greater number of low cloud tops for the DualM case, and more numerous high cloud tops for the Tiedtke clouds.

5.2 Maps

Figure 7 shows maps of the observed and model frequency of occurrence of trade cumulus samples on a $2^\circ \times 2^\circ$ latitude-longitude grid. The darker shades in the model figures clearly show the higher frequency of occurrence, but patterns are similar to the observations. Areas with low frequency of occurrence generally correspond to the stratocumulus regions or regions where deep convection frequently obscures the view of the lidar. Maps for the other Julys look very similar, while the maps for January reflect the seasonal shift of the ITCZ and the changes in the extent of the stratocumulus regions (not shown).

While the total number of TCu samples in the region is sufficient for robust distributions as shown in the previous figures, the noisy nature of the maps indicates that a month of observations is not sufficient for reliable statistics at any given grid point on the map.

To summarize: all versions of the model heavily overestimate the frequency of occurrence of TCu samples, but underestimates sample cloud fraction. With the Tiedtke parameterization for shallow convection, cloud top heights are often too high by several hundreds of meters, while the DualM scheme produces cloud tops in much

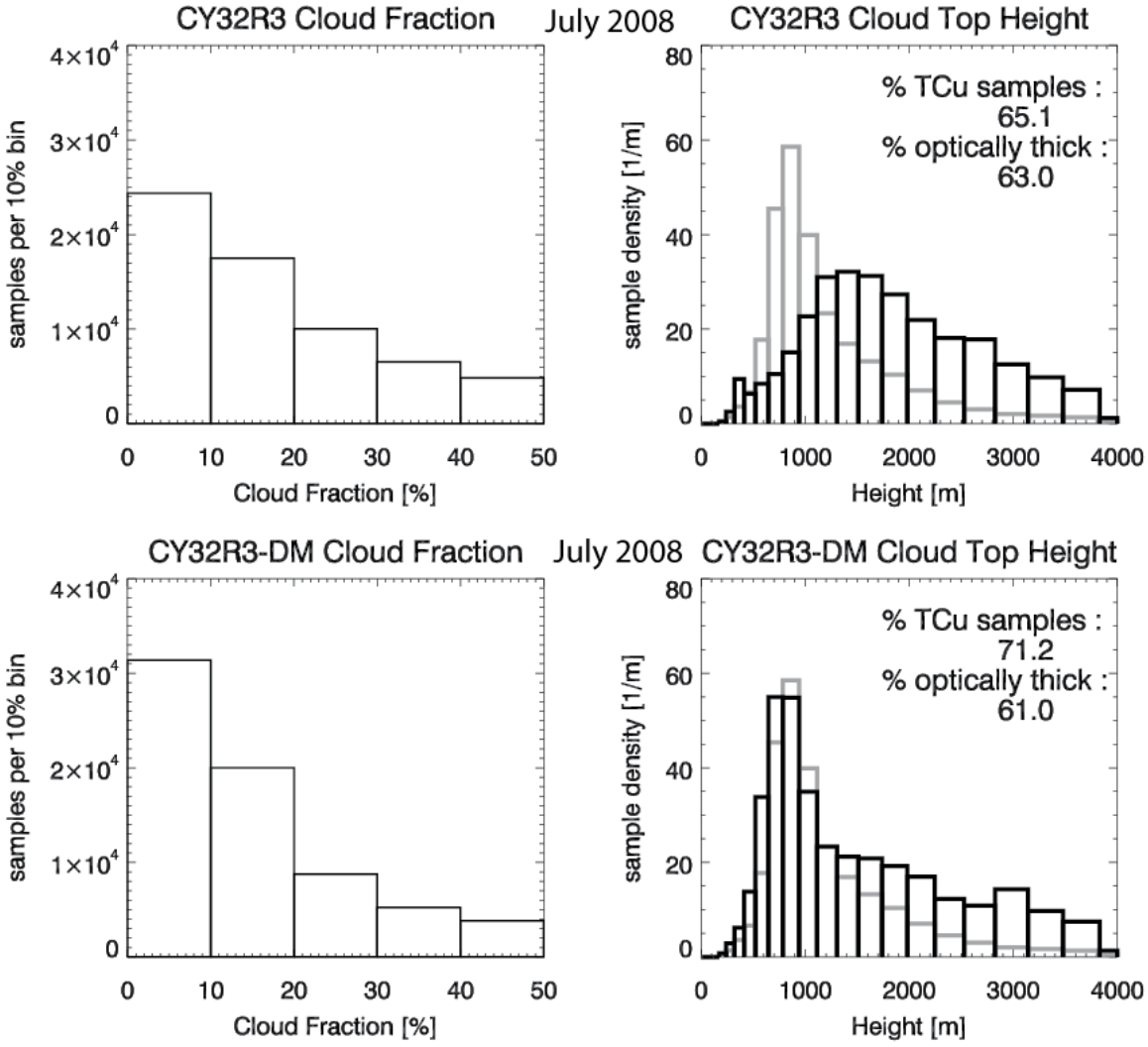

Figure 3: As in Fig. 2, but for model cycles CY32R3 and CY32R3-DM, July 2008.

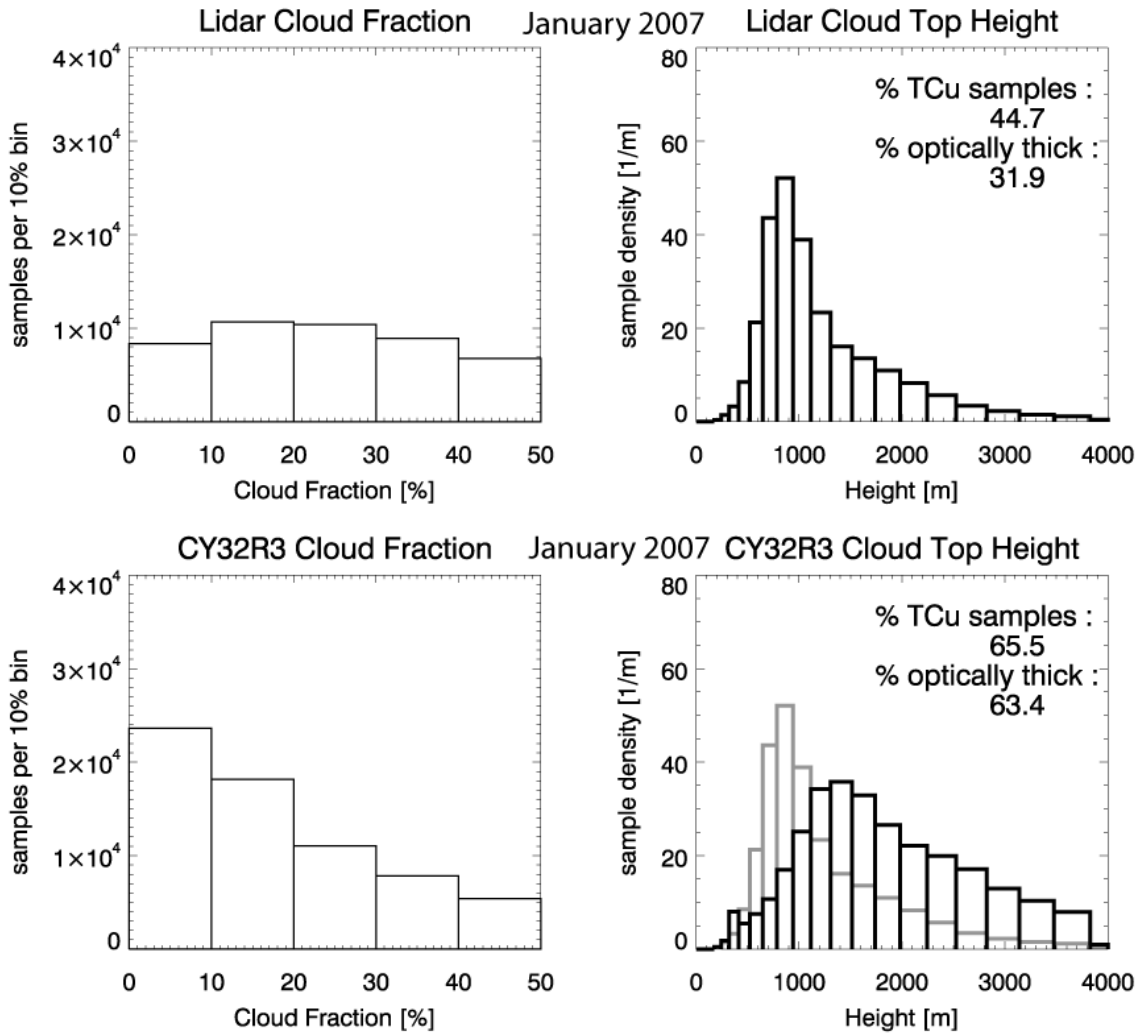

Figure 4: Cloud fraction and top height histograms for January 2007 from CALIPSO and CY32R3

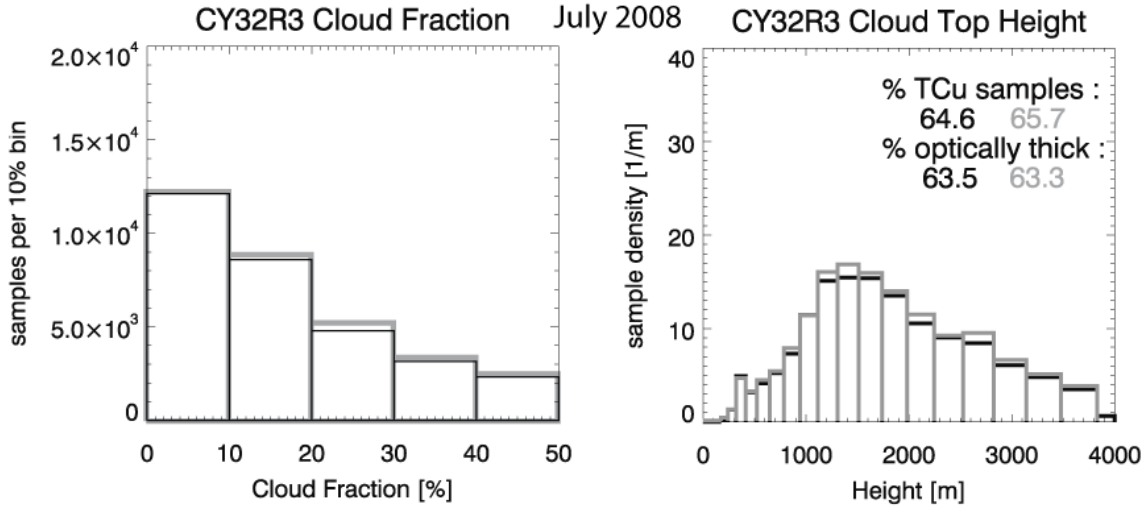

Figure 5: Cloud fraction and top height distributions for trade cumulus samples from model cycle CY32R3 during July 2008. Sample distributions from even days of the month, corresponding to model forecast hours 24-48, are shown in black, while distributions from odd days (forecast hours 48-72) are shown in grey.

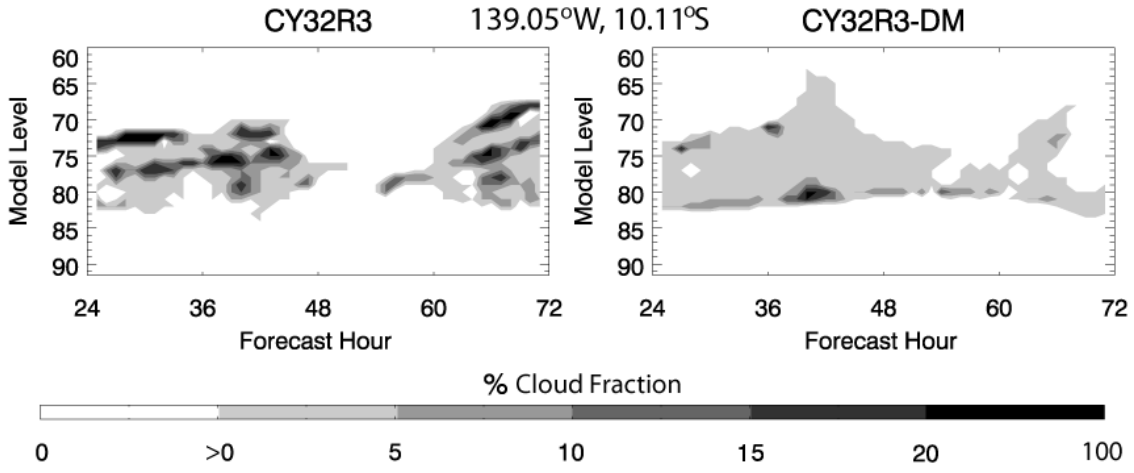

Figure 6: Hourly output of the model's cloud fraction from one grid point at 139.05°*W*, 10.11°*S. Left: From IFS with Tiedtke parameterization for shallow convection. The highest cloud fractions can be found in the upper half of the cloud. Right: From the IFS with DualM parameterization. Cloud fractions tend to be lower overall, with the highest values near cloud base. The cloud field is less noisy.*

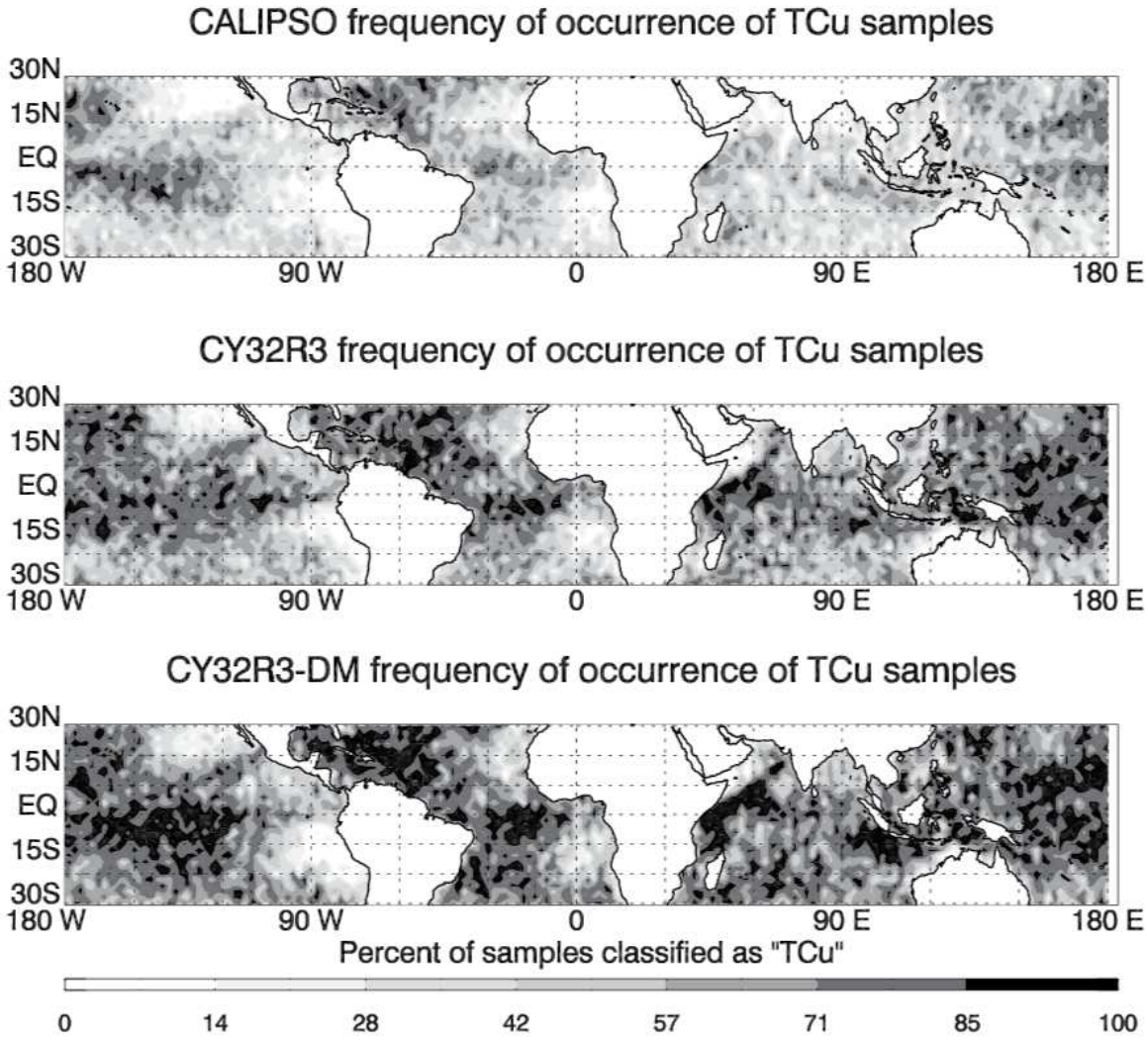

Figure 7: Maps of trade cumulus sample frequency of occurrence from CALIPSO, and from model cycles CY32R3 and CY32R3-DM for July 2008.

better agreement with observations. The modeled clouds are optically thick, such that twice as many samples are fully attenuated in the model compared to observations.

The question remains whether the model overall over- or underestimates the cloud cover in the trade cumulus regions. A simple multiplication of the sample cloud fractions with their frequency of occurrence will not yield a satisfactory answer, since it is unknown what, if any, cloud is present when the sample does not meet the trade cumulus criteria. Figure 8 shows monthly mean total cloud cover from MODIS Aqua, ISCCP, CALIPSO and the IFS. The level 3 Aqua MODIS monthly global product is used for this figure, as well as the ISCCP D2 climatological summary product (Rossow and Schiffer, 1999). Comparing model to CALIPSO, the model actually appears to be lacking cloud cover in the subtropical highs, particularly in the south Indian and Atlantic oceans. The additional clouds that CALIPSO observes could well be sub-visible high clouds, but MODIS, which does not have the same sensitivity to optically thin clouds as the lidar, also observes a higher total cloud cover in the trade cumulus regions. The ISCCP product has a lower cloud cover than the model and either of the other observational data sets in the Pacific ocean, but similar cloud cover in other areas. Cycles CY31R3 and CY32R3 have very similar total cloud cover, while the DualM parameterization produces a slightly reduced total cloud cover. This comparison of monthly mean maps is rather superficial, but the fact that the model's cloud cover falls within the range of various observational data sets is encouraging and suggests that model's overestimated frequency of occurrence must in large part be compensated by the low cloud fractions of the trade cumulus samples. The modeled clouds also appear to have a greater radiative impact (due to larger optical depth) than observed, which may further compensate for a lack of cloud, if the CALIPSO and MODIS figures are to be trusted. The model is well tuned to produce realistic radiative fluxes in the time mean.

5.3 Error sources

While the lidar can very accurately observe the vertical location of clouds, it is less than ideal for estimating the cloud fraction of an area (grid box). When using the lidar observations to estimate cloud fraction, the following two error sources should be considered:

Attenuation error

Part of the atmosphere cannot be observed due to signal attenuation. This is a limitation of the instrument, and the areas that cannot be observed must be excluded from the comparison with model data. By using the lidar simulator to correct for signal attenuation, this error component has been addressed. Nevertheless, there are many parametric choices to be made in the simulator (explored for example in Chiriaco et al. (2006) and Wilkinson et al. (2008)) which have the potential to introduce inaccuracies. Also, a systematic error in either cloud occurrence or optical thickness of high clouds will have an impact on the amount of low cloud that is excluded from the comparison based on the level of full attenuation calculated by the simulator.

Sampling error

The lidar only observes along a narrow track, rather than sampling the full area covered by a grid box. In the absence of a conceptual method to quantify this error, imaging observations from Aqua MODIS can provide an empirical estimate. From the 1 km resolution MODIS cloud mask, all points falling into a T399 model grid box are identified. A grid box has dimensions of approximately 50 km by 50 km. The ratio of cloudy to total pixels within this box provides a two-dimensional (area, 2D) cloud cover estimate. By identifying those pixels within the box closest to the lidar track, a one-dimensional (along-track, 1D) cloud cover can also be

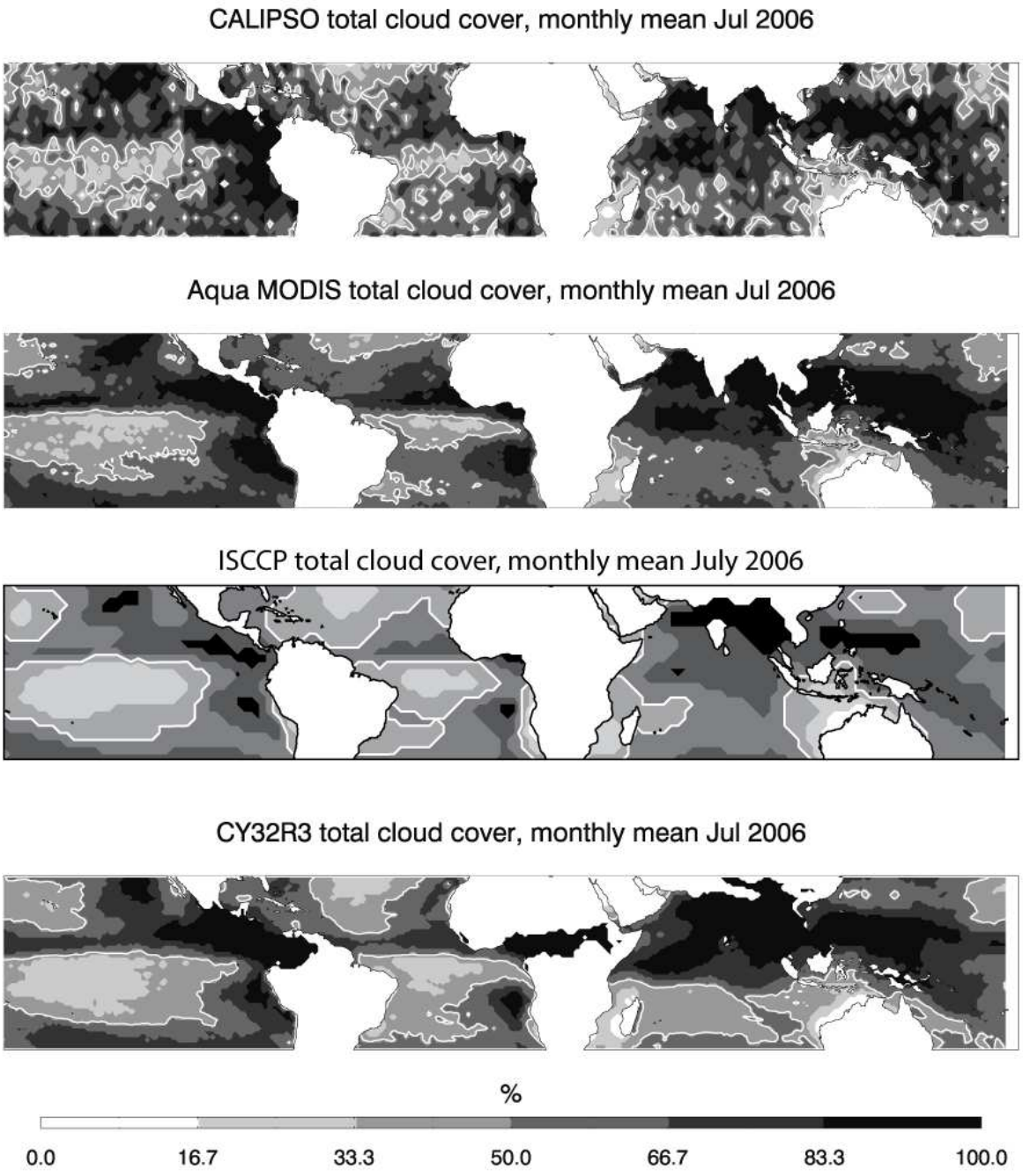

Figure 8: Maps of monthly mean total cloud cover from CALIPSO, Aqua MODIS, ISCCP and the model for the month of July 2006. The white solid contour marks the 50% level.

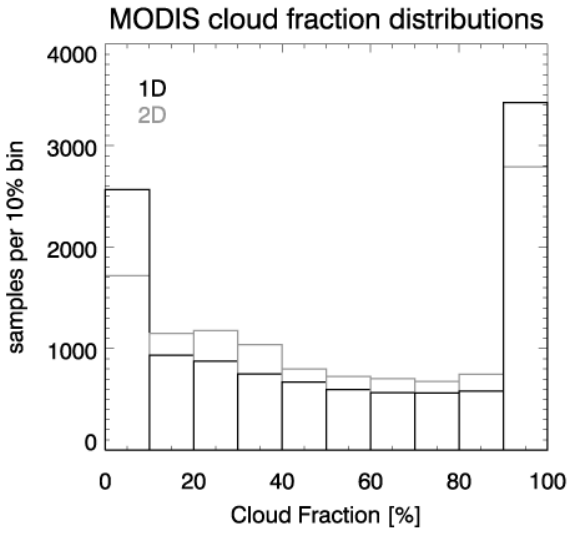

Figure 9: Cloud fraction distributions for MODIS cloud mask sampled within a grid box (grey, 2D) and along the CALIPSO track (black, 1D) from July 1st to July 8th 2008. Only ocean samples between $30^{\circ}N$ *and* $30^{\circ}S$ *are considered. Samples where CALIPSO detects high clouds are excluded. The difference between 1D and 2D distributions provides an empirical estimate of the sampling error for low clouds in the tropical and subtropical oceans.*

calculated. Since both 1D and 2D cloud cover are based on the same 1 km MODIS cloud mask, a comparison will show purely the error introduced by sampling the cloud fraction in a grid box along a track. Eight days of observations are used to produce the Figure 9 (July 1st to 8th 2008), corresponding to just over 6,000 grid points with good MODIS data. Only ocean grid points between $30^{\circ}N$ and $30^{\circ}S$ were used, and grid points with high clouds present were excluded based on CALIPSO cloud tops. Thus, while the area considered is the same as for the CALIPSO evaluation, all low cloud samples are included regardless of cloud fraction.

Figure 9 shows that for the 1D cloud fraction estimate, more samples fall into the lowest and highest cloud fraction bins. Most of these samples are either cloud free or are overcast. Fewer samples fall into the mid-range of the distribution compared to the 2D observations. For each calculated cloud fraction sample, the 2D estimate uses many more pixels (approximately 50^2) compared to the along-track estimate (approximately 50). This alone will make it less probable that completely clear or cloudy grid boxes will be observed in the 2D case.

Shown in Fig. 10 (left panel, solid black bars) is the CALIPSO cloud fraction distribution from Fig. 1 for July 2008. While cloud-free samples were excluded previously, this figure includes all samples that are cloud free below 4km in the lowest bin. The right panel shows the equivalent distribution for CY32R3 of the IFS. In both cases, adding the cloud free samples does increase sample numbers in the lowest cloud fraction bin, but both total sample number, and sample numbers at the low end of the cloud fraction range remain higher in the model compared to the CALIPSO observations.

Even though care was taken to choose MODIS samples similar to the CALIPSO trade cumulus samples, the two instruments will observe slightly different cloud fields. CALIPSO's 1 km shots are in fact the average of three individual lidar footprints, rather than covering a 1 km square area. While the MODIS cloud mask shows vertically integrated cloud cover, CALIPSO's TCu cloud fraction is based on low clouds only. Consequently, the relation of the observed 1D CALIPSO cloud fraction distribution to the unknown "true" distribution if the lidar where to sample the full area will likely differ slightly from what is shown in Fig. 9 for MODIS. Still, it seems reasonable that CALIPSO will also overestimate cloud free and overcast occurrences, and underestimate the occurrence of cloud fractions in the mid-range.

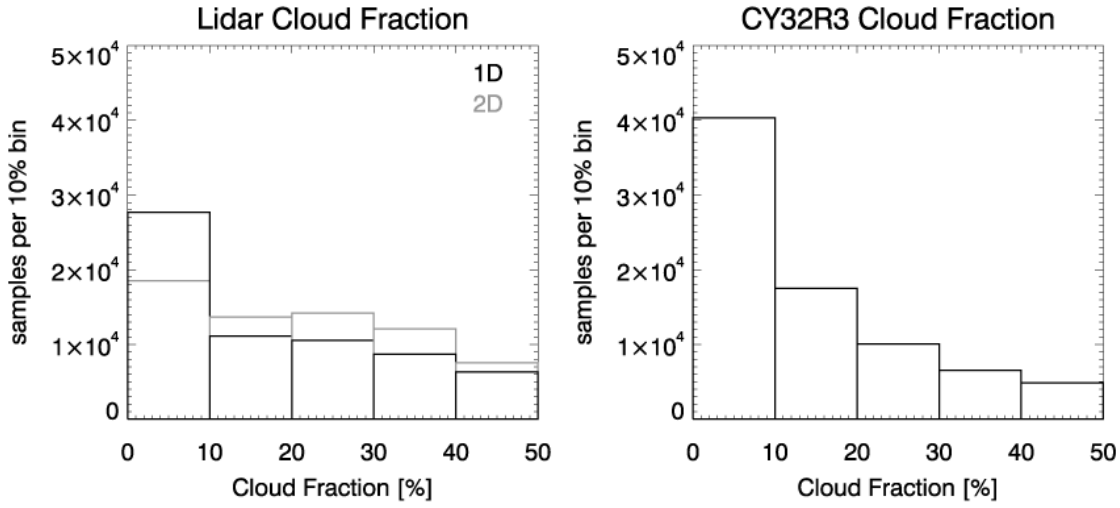

Figure 10: Cloud fraction distributions from (left) CALIPSO and (right) CY32R3 of the IFS. The left-most bin includes samples that are cloud-free below 4 km. Shown in grey is the CALIPSO distribution corrected for the sampling error, based on 1D vs. 2D cloud fraction comparison performed with MODIS cloud mask.

Shown as grey bars in Fig. 10 (left panel) is the CALIPSO cloud fraction distribution corrected for the sampling error based on the quotient of 2D MODIS samples to 1D MODIS samples. This correction is not accurate, but indicates the direction in which the CALIPSO distribution is likely to shift if the sampling error were removed: Fewer samples in the lowest bin, but more samples with higher cloud fractions.

While we can still not properly quantify the sampling error, the comparison of MODIS 1D to 2D cloud fractions indicates that qualitatively, the sampling error will shift the trade cumulus cloud fraction distribution towards higher values. Thus, the discrepancies between model and CALIPSO cloud fraction distributions can not be explained by the sampling error. In fact, the sampling error would act to lessen the differences.

6 Conclusions

CALIPSO observations prove to be highly useful in the assessment of the vertical location of trade cumulus clouds. The IFS with the physics package as used in the interim ECMWF re-analysis overestimates the typical cloud top height of trade cumulus clouds by 500 m and more. Updates to the Tiedtke convection parameterization and to the vertical diffusion do not have much impact on the trade cumulus clouds. The introduction of the DualM parameterization however leads to a dramatic improvement in the location of cloud top heights, and to a more realistic profile of cloud fraction.

The components of the model important for radiative balance in the trade cumulus areas are well tuned. Three of these components, cloud frequency of occurrence, cloud amount when present, and cloud optical depth, do not agree well with CALIPSO observations individually, but together compensate to produce reasonable mean cloud cover and radiative fluxes at the top of the atmosphere. In particular, all model versions tend to underestimate the grid box cloud fraction when trade cumulus is present, but compensate with a higher frequency of occurrence. This compensation illustrates the difficulties in updating individual components of the model's parameterization: all parts contributing to the balance must be addressed simultaneously, or the model performance will suffer.

By classifying clouds from a large area and considering the population's characteristics, a single month of observations is sufficient to provide a robust sample size. Cloud top height and fraction distributions for these populations do not differ appreciably from year to year or for different seasons.

This evaluation is limited to the frequency and extend of trade cumulus clouds in the model, as these are the aspects of shallow convection that the lidar can observe. Clearly, cloud amount and occurrence are not the only benchmarks for evaluating shallow convection parameterizations, and additional evaluations of convective transport and state of the atmosphere are necessary to assess the overall performance of a parameterization.

Acknowledgements

The development and testing of the DualM parameterization in the IFS model is supported by a fellowship from the Atmospheric Radiation Measurement program at ECMWF (Grant No. DE-FG02-07ER64400). The ISCCP D2 data were obtained from the International Satellite Cloud Climatology Project web site http://isccp.giss.nasa.gov maintained by the ISCCP research group at the NASA Goddard Institute for Space Studies, New York, NY. in May 2009. The CALIPSO 1 km cloud layer product, versions 2.01 and 2.02, was retrieved from the Atmospheric Science Data Center at the NASA Langley Research Center. MODIS data were obtained through the Level 1 and Atmosphere Archive and Distribution System (LAADS) web service.

Appendix

The Dual Mass Flux parameterization as documented in Neggers et al. (2009) and Neggers (2009) is modified in the following way for the IFS CY32R3-DM discussed in this article:

(1) Wind errors are reduced and model scores improve when momentum transport by shallow cumulus convection is accounted for (Tiedtke, 1989). This transport is approximated using the conventional entraining parcel/mass-flux approach without pressure gradient term.

(2) The eddy-diffusivity component within layers containing shallow cumulus clouds is written as a function of stability using a Richardson number formulation just as in the statically stable atmosphere(Bechtold et al., 2008).

(3) The modified Tiedtke scheme, as used in the operational IFS, permits triggering above the surface layer(Bechtold et al., 2004), which is most commonly found in frontal convection. Currently, the DualM scheme only replaces the Tiedtke convection for shallow clouds originating in the surface layer, while the Tiedtke scheme continues to address convection trigged above.

(4) Derbyshire et al. (2004) demonstrate the large impact of environmental humidity on cumulus activity. The concept of convective premoistening suggests a mechanism whereby earlier convective updrafts moisten the environment locally, which favours the growth of later updrafts. Since such small scale moisture variations are not explicitly resolved on the model grid, we can take advantage of the prognostic total water variance equation in the DualM shallow convection scheme to implement premoistening. The parcel entrainment is then written as

$$\frac{\partial q_{up}}{\partial z} = -\varepsilon \left(q_{up} - q_{env} \right)$$

where q_{env} corresponds to the mean of the top tail of a gaussian moisture distribution with total water variance σq_t^2. The tail limit is currently choosen as the top 10%. Further testing with LES is needed to validate this limit.

The DualM parameterization uses large entrainment rates in agreement with LES simulations and observations (Nitta, 1975; Siebesma et al., 2003). Yet, through convective preconditioning, we manage to maintain sufficiently strong convective transport, which is conventionally only achieved through unrealistically small entrainment rates.

References

Ahlgrimm, M., D. Randall, and M. Köhler, 2009: Evaluating cloud frequency of occurrence and top height using space-borne lidar observations. *Mon. Wea. Rev.*, **137**, 4225–4237.

Bechtold, P., J. Chaboureau, A. Beljaars, A. Betts, M. Köhler, M. Miller, and J. Redelsperger, 2004: The simulation of the diurnal cycle of convective precipitation over land in a global model. *Quart. J. Roy. Meteor. Soc.*, **130**, 3119–3137, doi:10.1256/qj.03.103.

Bechtold, P., M. Köhler, T. Jung, F. Doblas-Reyes, M. Leutbecher, M. Rodwell, F. Vitart, and G. Balsamo, 2008: Advances in simulating atmospheric variability with the ECMWF model: From synoptic to decadal time-scales. *Quart. J. Roy. Meteor. Soc.*, **134**, 1337–1352.

Beljaars, A., P. Bechtold, M. Köhler, A. Orr, and A. Tompkins, 2006: Developments in model physics after ERA-40. *ECMWF/GEO workshop on atmospheric reanalysis*, European Centre for Medium-Range Weather Forecasts, Reading, UK, 81–90.

Chiriaco, M., R. Vautard, H. Chepfer, M. Haeffelin, J. Dudhia, Y. Wanherdrick, Y. Morille, and A. Protat, 2006: The Ability of MM5 to Simulate Ice Clouds: Systematic Comparison between Simulated and Measured Fluxes and Lidar/Radar Profiles at the SIRTA Atmospheric Observatory. *Mon. Wea. Rev.*, **134**, 897–918.

Derbyshire, S., I. Beau, P. Bechtold, J. Grandpeix, J. Piriou, J. Redelsperger, and P. Soares, 2004: Sensitivity of moist convection to environmental humidity. *Quart. J. Roy. Meteor. Soc.*, **130 (604)**, 3055–3080.

Iacono, M., J. Delamere, E. Mlawer, M. Shephard, S. Clough, and W. Collins, 2008: Radiative forcing by long-lived greenhouse gases: Calculations with the AER radiative transfer models. *J. Geophys. Res.*, **113**, D13 103, doi:10.1029/2008JD009944.

Jakob, C., 1999: Cloud Cover in the ECMWF Reanalysis. *J. Climate*, **12**, 947–959.

Jakob, C., 2003: An improved strategy for the evaluation of cloud parameterizations in GCMs. *Bull. Amer. Meteor. Soc.*, **84**, 1387–1401.

Jung, T., et al., 2009: The ECMWF model climate: Recent progress through improved physical parameterizations. *ECMWF Seminar on Parameterization of Subgrid Physical Processes*, European Centre for Medium-Range Weather Forecasts, Reading, UK.

Köhler, M., 2005: Improved prediction of boundary layer clouds. *ECMWF Newsletter*, **104**, 18–22.

Neggers, R., 2009: A Dual Mass Flux Framework for Boundary Layer Convection. Part II: Clouds. *J. Atmos. Sci.*, **66**, 1489–1506.

Neggers, R., M. Khler, and A. Beljaars, 2009: A Dual Mass Flux Framework for Boundary Layer Convection. Part I: Transport. *J. Atmos. Sci.*, **66**, 1465–1487.

Nitta, T., 1975: Observational determination of cloud mass flux distributions. *J. Atmos. Sci.*, **32 (1)**, 73–91.

Räisänen, P., H. Barker, M. Khairoutdinov, J. Li, and D. Randall, 2004: Stochastic generation of subgrid-scale cloudy columns for large-scale models. *Quart. J. Roy. Meteor. Soc.*, **130**, 2047–2067, doi:10.1256/qj.03.99.

Rossow, W. and R. Schiffer, 1999: Advances in Understanding Clouds from ISCCP. *Bull. Amer. Meteor. Soc.*, **80**, 2261–2287.

Siebesma, A., et al., 2003: A Large Eddy Simulation Intercomparison Study of Shallow Cumulus Convection. *J. Atmos. Sci.*, **60**, 1201–1219.

Simmons, A., S. Uppala, D. Dee, and S. Kobayashi, 2007: ERA-Interim: New ECMWF reanalysis products from 1989 onwards. *ECMWF Newsletter*, **110**, 25–35.

Tiedtke, M., 1989: A Comprehensive Mass Flux Scheme for Cumulus Parameterization in Large-Scale Models. *Mon. Wea. Rev.*, **117**, 1779–1800.

Tiedtke, M., 1993: Representation of Clouds in Large-Scale Models. *Mon. Wea. Rev.*, **121**, 3040–3061.

Tompkins, A., et al., 2004: *Moist physical processes in the IFS: progress and plans*. European Centre for Medium-Range Weather Forecasts Technical Memo No. 452.

Uppala, S., et al., 2005: The ERA-40 re-analysis. *Quart. J. Roy. Meteor. Soc.*, **131**, 2961–3012.

Vaughan, M., D. Winker, and K. Powell, 2005: *CALIOP Algorithm Theoretical Basis Document, Part 2: Feature Detection and Layer Properties Algorithms*. NASA Langley Research Center, PC-SCI-202 Part 2, Release 1.01 pp.

Wilkinson, J., R. Hogan, A. Illingworth, and A. Benedetti, 2008: Use of a Lidar Forward Model for Global Comparisons of Cloud Fraction between the ICESat Lidar and the ECMWF Model. *Mon. Wea. Rev.*, **136**, 3742–3759.